Am J Physiol Gastrointest Liver Physiol 329: G628–G638, 2025.
First published October 10, 2025; doi:10.1152/ajpgi.00362.2024

american physiological society

AMERICAN JOURNAL OF PHYSIOLOGY
GASTROINTESTINAL AND LIVER PHYSIOLOGY

RESEARCH ARTICLE

N-glycans on SLC26A3 do not significantly alter plasma membrane or lipid raft trafficking, but appear to stabilize interdomain contacts to stimulate transport

Sophie Achilles,[1] Jan-Niklas Tomczak,[2] Fabiane-Samira Baumann,[1] Bassam G. Haddad,[3,4] Stefan Oswald,[5] Jan-Philipp Machtens,[3,4] Eric R. Geertsma,[6] Ilka Wittig,[2] and Georg Lamprecht[1]

[1]*Division of Gastroenterology, Hepatology and Nutritional Medicine, Department of Internal Medicine, Rostock University Medical Center, Rostock, Germany;* [2]*Functional Proteomics Group, Institute for Cardiovascular Physiology, Goethe University, Frankfurt, Germany;* [3]*Institute of Biological Information Processing (IBI-1), Molekular- und Zellphysiologie, and JARA-HPC, Forschungszentrum Jülich, Jülich, Germany;* [4]*Institute of Neurophysiology, Hannover Medical School, Hannover, Germany;* [5]*Institute of Pharmacology and Toxicology, Rostock University Medical Center, Rostock, Germany; and* [6]*Max Planck Institute of Molecular Cell Biology and Genetics, Dresden, Germany*

Abstract

DRA (Downregulated in adenoma, SLC26A3) is a major apical intestinal Cl^-/HCO_3^- exchanger, which is expressed in complex and hybrid *N*-glycosylated forms. Although the importance of *N*-glycosylation is evident from the significantly reduced transport activity of non-*N*-glycosylated DRA constructs (DRA-N0), the underlying molecular mechanisms are controversial. Therefore, plasma membrane expression and lipid raft localization of glycosylation-deficient DRA-N0 were analyzed in HEK cells. The activity of DRA-N0 was reduced by 70% compared with the wild-type construct. Absolute expression of DRA-N0 was significantly reduced by ~57% in the cell lysate and by 34 and 45% in the plasma membrane and in plasma membrane-derived lipid rafts, respectively. These amounts are insufficient to account for the reduction in activity. Furthermore, the statistical analysis did not support a difference in the relative expression of DRA and DRA-N0 in the plasma membrane and in plasma membrane-derived lipid rafts, indicating that *N*-glycosylation does not affect transport activity through trafficking and localization in these cell compartments. To gain insight into potential intramolecular effects of *N*-glycosylation on DRA, its three-dimensional structure was predicted using AlphaFold3 with complex *N*-glycans covalently attached to N153, N161, and N164 in the transport domain. This revealed multiple inward- and outward-facing conformations of the protein. The number of interdomain contacts of the transport domain-bound glycans with the scaffold domain was higher in the inward-facing state. Because substrate release to the cytoplasm represents the rate-limiting step in many transport proteins, this suggests that in DRA, glycans stabilize the inward-facing state facilitating anion transport.

NEW & NOTEWORTHY Deficient *N*-glycosylation decreases DRA transport activity but does not significantly affect trafficking to the plasma membrane or to lipid rafts. Meanwhile, molecular modeling predicts stabilizing interdomain contacts of the glycans, covalently attached to the transport domain, with the scaffold domain having more contacts in the inward-facing state. Favoring the inward-facing state may facilitate more efficacious anion transport, as substrate release from this state into the cytoplasm is a rate limiting step for numerous transport proteins.

glycosylation; lipid rafts; plasma membrane trafficking; SLC26A3; structure prediction

INTRODUCTION

Downregulated in adenoma (DRA, SLC26A3) is a Cl^-/HCO_3^- exchanger and is located primarily in the apical membrane of intestinal epithelial cells in the ileum and colon as well as in the duodenum (1). The physiological importance is evident by a naturally occurring loss-of-function mutation that causes congenital chloride-losing diarrhea (CLD) manifested as massive diarrhea requiring lifelong fluid and salt supplementation (2, 3). The disease is also mimicked in DRA knockout mice (4). Given its quantitative importance in fluid absorption from the intestine, tight regulation of DRA activity is believed to be required to maintain fluid homeostasis and has been studied along that line. Initially, DRA was thought to function entirely in parallel with the intestinal Na^+/H^+ exchanger NHE3 to mediate NaCl absorption (5–7). However, DRA is also expressed in some intestinal segments without NHE3, indicating additional functions—mainly bicarbonate secretion, which at least partly requires the presence of CFTR (8–10). In addition to mediating ion transport, the physiological role of DRA involves indirect mechanisms such as maintaining the pH of the mucus covering the

Correspondence: G. Lamprecht (georg.lamprecht@med.uni-rostock.de).
Submitted 19 November 2024 / Revised 8 December 2024 / Accepted 1 October 2025

epithelium, which in turn, is a major determinant of the intestinal microbiome with its pro- or anti-inflammatory impact on intestinal physiology and pathology (11).

DRA is a member of the SLC26 family of anion transporters. The structures of several other members of the SLC26 family (SLC26A4, SLC26A5, SLC26A6, and SLC26A9) have been experimentally resolved and so far exhibit remarkable similarity, with a characteristic domain-swapped dimer, a cytoplasmic domain, and a transmembrane domain (TMD). The TMD is composed of a static scaffold domain and a relatively mobile transport domain that binds an anion and carries it to the opposite side of the membrane through a putative elevator-like mechanism (12).

The activity of any plasma membrane (PM) transporter, including DRA, is determined by the solute transport rate of the individual transport protein and the number of these proteins in the PM. Currently, most studies show that DRA activity changes as a result of the number of transporters in the PM, the insertion into lipid rafts (LRs), and the coupling to CFTR and maybe also NHE3. The number of DRA transporters in the cell membrane is determined by insertion into and retrieval from the plasma membrane as well as constitutive and regulated endosomal recycling. Disruption of LRs by methyl-β-cyclodextrin (MβCD) leads to incomplete inhibition of DRA activity (13). Also of note, the coupling to CFTR or NHE3 may require direct interaction and/or functional activity of either of these transporters (10, 14).

Recycling of DRA involves the interaction of its C-terminal PDZ interaction motif ETKF (Glutamate, Threonine, Lysine, Phenylalanine) with PDZ adaptor proteins (6). In a PDZ-dependent pathway, DRA can be recycled to the PM via rab11-positive recycling endosomes (15). In addition, DRA can be recycled directly from early endosomes into the PM through interaction with the PDZ adaptor protein SNX27 and the retromer complex (16). Within the PM, DRA is particularly active when localized in LRs (13). The incorporation of DRA into LRs is likewise facilitated by the interaction with PDZ adaptor proteins and occurs along a PI3 kinase-dependent exocytosis pathway (13).

Similar to most proteins of the SLC26 family, DRA undergoes *N*-glycosylation. Glycosylation is the primary posttranslational modification in mammals, with *N*-glycosylation being of particular importance (17). This process predominantly occurs in the ER and Golgi. After "en bloc" transfer of the *N*-glycan to asparagine residues in the ER, *N*-glycans mature into complex forms in the Golgi through the addition of sugars, elongation of branching *N*-acetylglucosamine residues, and capping of elongated branches (17). This results in different forms of *N*-glycosylation, with DRA being expressed both as a hybrid *N*-glycosylated form and as a complex *N*-glycosylated form (18, 19). The relevance of *N*-glycosylation for DRA is evident, as DRA has significantly reduced activity when *N*-glycosylation is abrogated (18, 20). Although no naturally occurring, CLD-causing DRA mutations are known that directly affect its *N*-glycosylation sites, several mutations are known that result in varying degrees of impaired *N*-glycosylation (20).

Previously, we and others have shown that DRA is highly active in LRs and that the complex *N*-glycosylated form of DRA is highly prevalent in LRs (13, 21). In addition, raft association of other membrane proteins is enhanced by intact *N*-glycosylation (22–24). Therefore, we have characterized the importance of *N*-glycosylation of DRA for its activity and its presence in the PM, LRs, and plasma membrane-derived lipid rafts (PM-LRs). In addition, we used structure prediction of DRA to gain insight into potential intramolecular effects of DRA glycosylation.

MATERIALS AND METHODS

Cloning and Expression Constructs

An *N*-terminally EGFP (enhanced green fluorescent protein)-tagged DRA expression construct (pEGFP-DRA), previously described and used by us (25), was used to generate a glycosylation-deficient DRA expression construct. All four glycosylation sites (N153, N161, N164, and N165) were mutated from N to Q using Q5 site-directed mutagenesis kit according to the manufacturer's instructions (Cat. No. E0554S from NEB, Ipswich). Using two primers adopted from the study by Hayashi et al. (18) (fw: CAAAACTCGCAACAATCTTCACTACTGG, rv: AGGCAATCCCAAAGTAGTTGCTTGGCG), only three glycosylation sites were successfully altered (N161, N164, and N165). To mutate the remaining glycosylation site N153, the use of an additional primer pair was required (fw: CCTCAAAACTCGCAACAATCTTCACTACTGG, rv: CAATCCCAAAGTAGTTGCTTGGCGATCTGGG). The resulting construct, hereinafter referred to as pEGFP-DRA-N0, was sequenced to ensure correct cloning.

Cell Lines

HEK293 cells were used to generate stable single-cell clones of EGFP-DRA and EGFP-DRA-N0. Following transfection with TurboFectin 8.0 according to the instructions of the manufacturer, cells were seeded in 10 cm Petri dishes at densities of 1–1,000 cells/dish, and after 3–4 wk, single cell colonies were harvested using cloning cylinders. The resulting clonal cell lines were analyzed for protein expression by Western blot and for activity by fluorometry. Subsequently, one functional clone with comparable total DRA protein expression was selected for EGFP-DRA and EGFP-DRA-N0, respectively. All cell clones were cultured in DMEM with glucose (PAN Biotech, Aidenbach, Germany) supplemented with 10% FBS, 0.5% penicillin/streptomycin, and 250 μg/mL G418 (Roche, Basel, Switzerland).

SDS-PAGE and Western Blot

Cells were washed in PBS pH 7.4 and lysed in TBS (20 mM TRIS, pH 7.5, 150 mM NaCl) with 1% TritonX-100 and 1:10 protease inhibitor cocktail (cOmplete Mini, EDTA-free; Roche, Basel, Switzerland) by incubating for 30 min on ice and vigorously vortexing every 5 min. After centrifugation for 10 min at 4°C and 10,000 *g*, the supernatant was collected as protein lysate. Protein concentration was determined using Pierce BCA Protein Assay Kit (Cat. No. 23225 from Thermo Scientific, Waltham).

Unless indicated otherwise, 50 μg of protein was denatured in SDS-PAGE sample buffer (250 mM TRIS, 280 mM SDS, 40% vol/vol Glycerol, 100 mM DTT, pH 6.8) for 30 min at 60°C, separated by 7% SDS-PAGE and tank blotted overnight onto PVDF membrane. Membranes were blocked in Blocking Buffer for Fluorescent Western Blotting (MB-070

from Rockland Immunochemicals, Limerick) diluted 1:3 in TBS-T (20 mM TRIS, pH 7.5, 150 mM NaCl, 0.1% Tween 20). Primary antibody incubation was performed with anti-EGFP monoclonal antibody (RRID:AB_10013427, 1:1,000), anti-flotillin-1 monoclonal antibody (RRID:AB_2106563, 1:100), and/or anti-β-actin monoclonal antibody (RRID:AB_2223172, 1:1,000) in TBS-T for 4 h, followed by secondary antibody incubation with IRDye 800CW goat anti-mouse antibody (RRID:AB_621842, 1:5,000) and IRDye 680RD goat anti-rabbit antibody (RRID:AB_10956166, 1:5,000) in TBS-T for 30 min. Between each step, blots were washed five times with TBS-T. Imaging was done using the Image Studio software (RRID: SCR_015795) on the Li-Cor Odyssey CLx Imaging-System and for quantification of the bands, the ImageJ (RRID: SCR_003070) Gel Analyzer plugin was used. Full-length Western blots are presented in Supplemental Fig. S1.

Deglycosylation by PNGaseF

For PNGaseF treatment (Cat. No. P0704 from NEB, Ipswich), 9 μL of protein lysate (max. 20 μg of protein) were combined with 1 μL of glycoprotein denaturing buffer. After incubation at 60°C for 30 min, the mixture was cooled on ice and then reconstituted to a total reaction volume of 20 μL by adding 2 μL of GlycoBuffer 2 (10×), 2 μL of 10% NP-40, and an appropriate volume of H_2O. After the addition of 1 μL of PNGase F, the reaction was incubated at 37°C for 1 h. After combining with 20 μL of 2× SDS-PAGE sample buffer, samples were subjected to SDS-PAGE.

Fluorometry

DRA activity was measured as previously described as changes of the intracellular pH (pH_i) upon the removal and re-addition of extracellular chloride by BCECF fluorometry (25). The pH_i was determined using the Nigericin/high K calibration technique. The pH_i changes upon chloride removal were recorded and the initial slope was calculated by nonlinear curve fitting. The bicarbonate flux was calculated by multiplying the initial slope of alkalinization with the buffer capacity at the corresponding pH_i (26). All buffers contained 5 mM K-gluconate, 2 mM Mg-gluconate, 1 mM Ca-gluconate, 10 mM HEPES, and 10 mM glucose. The chloride-containing buffer was supplemented with 115 mM NaCl and 25 mM $NaHCO_3$, and the nonchloride buffer with 115 mM Na-gluconate and 25 mM $NaHCO_3$. Calibration buffers were supplemented with 100 mM KCl and 40 mM tetramethylammonium chloride.

Quantification of DRA Present in the Plasma Membrane

Cell surface biotinylation using the Pierce Cell Surface Biotinylation and Isolation Kit (Cat. No. 89881 from Thermo Scientific, Waltham) was applied to separate DRA present in the PM from intracellular compartments. Cells were cultured in T75 flasks, biotinylated for 30 min at 4°C with Sulfo-NHS-SS-Biotin, and after quenching and washing, lysed in 500 μL of lysis buffer completed with 1:10 protease inhibitor cocktail (cOmplete Mini, EDTA-free; Roche, Basel, Switzerland). After capturing the biotinylated cell surface proteins on NeutrAvidin Agarose beads and washing, elution from the beads was performed using 300 μL of SDS-PAGE sample buffer in two incubation steps, the first at room temperature for 60 min and the second at 95°C for 5 min. Samples of 20 μL each of the lysate and the supernatant after bead-binding, as well as 50 μL of the eluate, were separated on 7% SDS-PAGE (referred to in the figures as lysate, supernatant, and beads). After Western blot and quantification of the DRA bands using ImageJ, the percentage of DRA present on the cell surface was calculated. Only experiments with a recovery of 85%–115% DRA in supernatant plus beads versus the lysate were included in the final analyses.

Wheat Germ Agglutinin Colocalization

Alexa 350-labeled wheat germ agglutinin (WGA) conjugate was used to label the cell membrane and test for the colocalization with EGFP-DRA. Cells were seeded in μ-Slide 18 wells (Cat. No. 81816 from ibidi, Gräfelfing, Germany) and grown for 2–3 days to confluency. Cells were fixed with formaldehyde (4% in PBS pH 7.4) for 20 min at room temperature and blocked with 1% BSA in PBS pH 7.4 for 30 min at room temperature. Following incubation with Alexa 350-conjugated WGA (5 μg/mL; Cat. No. W11263 from Thermo Scientific, Waltham) in the dark for 1 h, the cells were mounted in liquid fluorescence mounting media (Cat. No. 50001 from ibidi, Gräfelfing, Germany). Slides were stored at 4°C in the dark until microscopic examination. Colocalization of Alexa 350-labeled WGA and endogenous EGFP-DRA fluorescence was visualized with a Zeiss LSM 780 microscope (excitation at 405 nm and 488 nm lasers, respectively) using a ×40 Plan-Neofluar objective with immersion oil. ZEN software (RRID: SCR_013672) was used for image display and processing, followed by processing and data analysis with ImageJ software. CZI files were imported into ImageJ as split channels, consistent background subtraction was used for all experiments and randomly selected individual cells were defined and examined in five to ten regions of interest (ROIs) for each experiment. Colocalization was assessed using the ImageJ plugin "Colocalization Threshold," which incorporates Coste's automatic thresholding method for background correction and determines the Pearson's correlation coefficient (PCC). The PCC was computed for all ROIs per experiment and an average PCC value was then derived as one data point.

Isolation of Detergent-Resistant Membranes

Isolation of detergent-resistant membranes was performed as described previously (13). Cells grown to confluency in a T175 flask were scraped into 12 mL of ice-cold PBS pH 7.4; 4 mL were used to generate a lysate, which was kept as a reference. The remaining 9 mL were used for the isolation of detergent-resistant membranes: The cells were spun and the pellet was homogenized with 10 strokes in a Dounce homogenizer in 2 mL of TNE buffer (25 mM TRIS, 150 mM NaCl, 5 mM EDTA, pH 7.5) with protease inhibitor cocktail and 1% Triton X-100. The homogenized material was mixed with an equivalent volume of 80% sucrose solution, transferred into a centrifuge tube, and then overlaid with 4 mL each of 30% and 5% sucrose in TNE buffer. After overnight centrifugation in a Beckman SW41Ti rotor at 190,000 *g*, twelve fractions were sampled from the top of the gradient. After determining the protein concentration, 50 μg of protein or, if too diluted, 900 μL of each fraction from the gradient were precipitated. For this, 1:150 of 2% sodium deoxycholate (f.c. 0.013%) were added, and samples were incubated for 10 min at RT. After

adding 1:15 of 100% trichloracetic acid (f.c. 6.67%), samples were again incubated for 20 min at 4°C and the precipitate was pelleted for 15 min at 10,000 *g* and 4°C. The pellets were washed three times with 1 mL of acetone and spun for 5 min at 10,000 *g* and 4°C. The final pellets were dissolved in 50 μL of SDS-PAGE sample buffer and subjected to SDS-PAGE.

Isolation of Plasma Membrane-Derived Lipid Rafts

Cells cultured to confluency in a T175 flask were scraped into 10 mL of ice-cold PBS pH 7.4; 2 mL were used to generate a lysate, which was kept as a reference. The remaining 8 mL were used to isolate PM-LRs using the Minute PM-Derived Lipid Raft Isolation Kit (Cat. No. LR-042 from Invent Biotechnologies, Plymouth) according to the instructions of the manufacturer. For quantification of DRA incorporation into PM-LRs, the resulting pellet was dissolved in 100 μL of SDS-PAGE sample buffer, and 10 μL of the lysate, and 50 μL of the dissolved pellet were subjected to SDS-PAGE.

For the liquid chromatography-tandem mass spectrometry (LC-MS/MS) measurement of DRA in the PM, the instructions were followed until the step of isolation of the PM (indicated in the manual as isolated PM fraction), and the resulting pellet was frozen at −20°C. For the LC-MS/MS measurement of DRA in PM-derived lipid rafts, the entire procedure was performed, and the resulting pellet was frozen at −20°C.

Targeted Proteomics

To measure the absolute protein abundance of DRA in the cells, a cell lysate was prepared as described in *SDS-PAGE and Western Blot*. The Minute PM-Derived Lipid Raft Isolation Kit was used as described earlier to obtain pellets of the PM and the PM-LRs, which were then dissolved in 150 μL of TBS (20 mM TRIS, pH 7.5, 150 mM NaCl) with 1% TritonX-100 and 1:10 protease inhibitor cocktail (cOmplete Mini, EDTA-free; Roche, Basel, Switzerland). The protein concentration of these samples was determined using the Pierce BCA Protein Assay Kit. They were digested by the filter-aided sample preparation (FASP) procedure (27). For this, the samples containing a maximum of 100 μg protein were diluted to 200 μL with UT buffer (8 M urea, 2 M thiourea) and applied to a cellulose membrane filter (Vivacon 500, 10,000 MWCO Hydrosart from Sartorius, Göttingen, Germany) pretreated with 1% formic acid. This was followed by incubation with 100 μL of 8 mM dithiothreitol at 56°C for 15 min, application of 100 μL of urea buffer (8 M urea, 100 mM TRIS, pH 8.5), incubation with 100 μL of 50 mM iodoacetamide at room temperature in the dark for 20 min, application of 100 μL of urea buffer, incubation with 100 μL of 8 mM dithiothreitol at 56°C for 15 min, application of 100 μL of urea buffer, and two applications of 100 μL of ABC buffer (65 mM ammonium bicarbonate, pH 7.8). After all steps, 30 min centrifugation was carried out at 14,000 *g* at RT. After overnight incubation with 100 μL of trypsin solution (0.01 μg/μL trypsin, 1% acetonitrile in ABC buffer; Sequencing Grade Modified Trypsin from Promega, Fitchburg), 10 μL of 10% formic acid was added and the eluate was kept as a sample after 10 min centrifugation. After adding 40 μL of ABC buffer, the eluate was sampled in the same tube after 10 min centrifugation.

The quantitative proteomic analyses were performed using liquid chromatography-tandem mass spectrometry (LC-MS/MS) targeted proteomics approach using stable-isotope labeled internal standards (28). Absolute quantification of DRA was achieved by monitoring the proteospecific peptide LIDAVGFSPLR. Na/K-ATPase was analyzed in parallel as a reference protein using the peptide LSLDELHR. Protein quantification was conducted on a 7500 QTRAP triple quadrupole mass spectrometer (AB Sciex, Darmstadt, Germany) coupled to an Agilent Technologies 1290 Infinity system (Agilent Technologies, Santa Clara). For each peptide, four mass transitions were monitored and the absolute protein abundance was assessed by using the stable isotope method. Details of the used chromatographic method have been described elsewhere (28). To ensure comparability between the samples, the DRA concentration was normalized to the individual sample protein content (pmol/mg protein).

Structure Predictions

To assess potential molecular mechanisms of glycosylation-enhanced transport activity, AlphaFold3 (AF3) (29) was used to make all-atom predictions of DRA (UniProt: P40879) with "Complex *N*-Glycan Cores." The AlphaFold3 server (29) was used to add glycosylations at N153, N161, and N164. A simplified "Complex *N*-Glycan" was chosen for prediction—glycosylation string used in AF3: NAG(NAG(MAN(MAN-(NAG)(NAG))(MAN(NAG)))). It is known that half of the DRA molecules carry mature complex *N*-glycan structures, whereas the remainder carry hybrid *N*-glycans (18), as opposed to high mannose *N*-glycans. As the absolute structure, or even the components of the mature *N*-glycan are currently unknown, we opted to perform our predictions in the presence of a complex *N*-glycan core structure, of which there are three that SLC proteins use (17)—di-, tri-, and tetra-antennary. The difference between these cores is the number of *N*-acetylglucosamine (GlcNAc) sugars attached to the branched mannose. Here, we used the tri-antennary core structure as a conservative and agnostic starting point. Six predictions were performed, each with a random seed, to generate 30 structures of the glycosylated DRA dimer. The resulting structures were clustered into two groups (inward-/outward-facing) according to the *Z*-height of the mobile transport domain relative to the static scaffold domain (Fig. 5*B*).

Contact analysis was performed to evaluate conformation-dependent (inward- vs. outward-facing) interdomain interactions of the glycans (covalently linked to the transport domain) and the scaffold domain. Two atom groups are defined as in contact when a heavy atom (i.e., not hydrogen) of the glycosylation comes within 10 Å of a backbone-Cα from a scaffold domain residue.

Images were rendered using VMD (30) and ChimeraX (31).

Statistical Analyses

Statistical analyses and plotting of experimental data were performed using GraphPad Prism 9. Assuming a normal distribution of all samples according to the Shapiro–Wilk test, *t* tests for independent samples were performed. Analyses of the fluorometry data were performed using JMP16 software according to the described algorithms (26). Interdomain

glycan contacts from AF3 predictions were calculated with in-house Python scripts. Due to unequal variances (Levene homogeneity test), the nonparametric Mann–Whitney *U* test was used.

Data are presented as means ± SD. $P < 0.05$ was considered statistically significant.

RESULTS

DRA Is Both Complex and Core/Hybrid *N*-Glycosylated

Protein expression and *N*-glycosylation of HEK/EGFP-DRA versus HEK/EGFP-DRA-N0 were assessed by Western blot (Fig. 1*A*). Two single-cell clones with comparable DRA protein expression according to Western blot results were selected. EGFP-DRA was observed as two bands with molecular weights of 120 and 160 kDa, with the upper band accounting for 53 ± 10% of the total intensity in the cell lysate. EGFP-DRA-N0 appeared as a single band of 110 kDa. After PNGaseF treatment, both bands of EGFP-DRA condensed to a single band of 110 kDa, indicating that the two bands are *N*-glycosylated. As expected, EGFP-DRA-N0 was not susceptible to PNGaseF treatment.

DRA is known to be expressed as a core/hybrid *N*-glycosylated and a complex *N*-glycosylated form, which is consistent with the fact that both EGFP-DRA bands are susceptible to PNGaseF treatment (18, 19). Thus, the larger 160 kDa DRA band is complex *N*-glycosylated DRA, whereas the smaller, 120 kDa band is core/hybrid *N*-glycosylated DRA and the 110 kDa band represents non-*N*-glycosylated DRA (deficient *N*-glycosylation).

DRA with Deficient *N*-Glycosylation Has Reduced Transport Activity

To detect changes in DRA activity, DRA-mediated changes of the intracellular pH (pH_i) were measured fluorometrically in HEK/EGFP-DRA (Fig. 1*D*) and HEK/EGFP-DRA-N0 cells (Fig. 1*E*) as well as in nontransfected HEK cells (Fig. 1*C*). DRA activity was induced by removal and readdition of extracellular chloride. Background corrected bicarbonate fluxes were calculated (Fig. 1*B*) and revealed that cells expressing EGFP-DRA display a much higher activity with a bicarbonate flux of 0.39 ± 0.14 mM/s compared with 0.09 ± 0.05 mM/s in EGFP-DRA-N0 expressing cells ($P = 0.0005$, $n = 6$). Thus, DRA with deficient *N*-glycosylation exhibits 70% reduced activity.

Wild-Type DRA and *N*-Glycosylation Deficient DRA Are Present at the Cell Surface

To detect differences in the surface expression of DRA, which could account for the reduction in activity, cell surface biotinylation was performed and wheat germ agglutinin (WGA) colocalization was tested (Fig. 2, *A* and *B*).

Using cell surface biotinylation 6.1 ± 3% of EGFP-DRA versus 7.6 ± 2% of EGFP-DRA-N0 was detected in the PM,

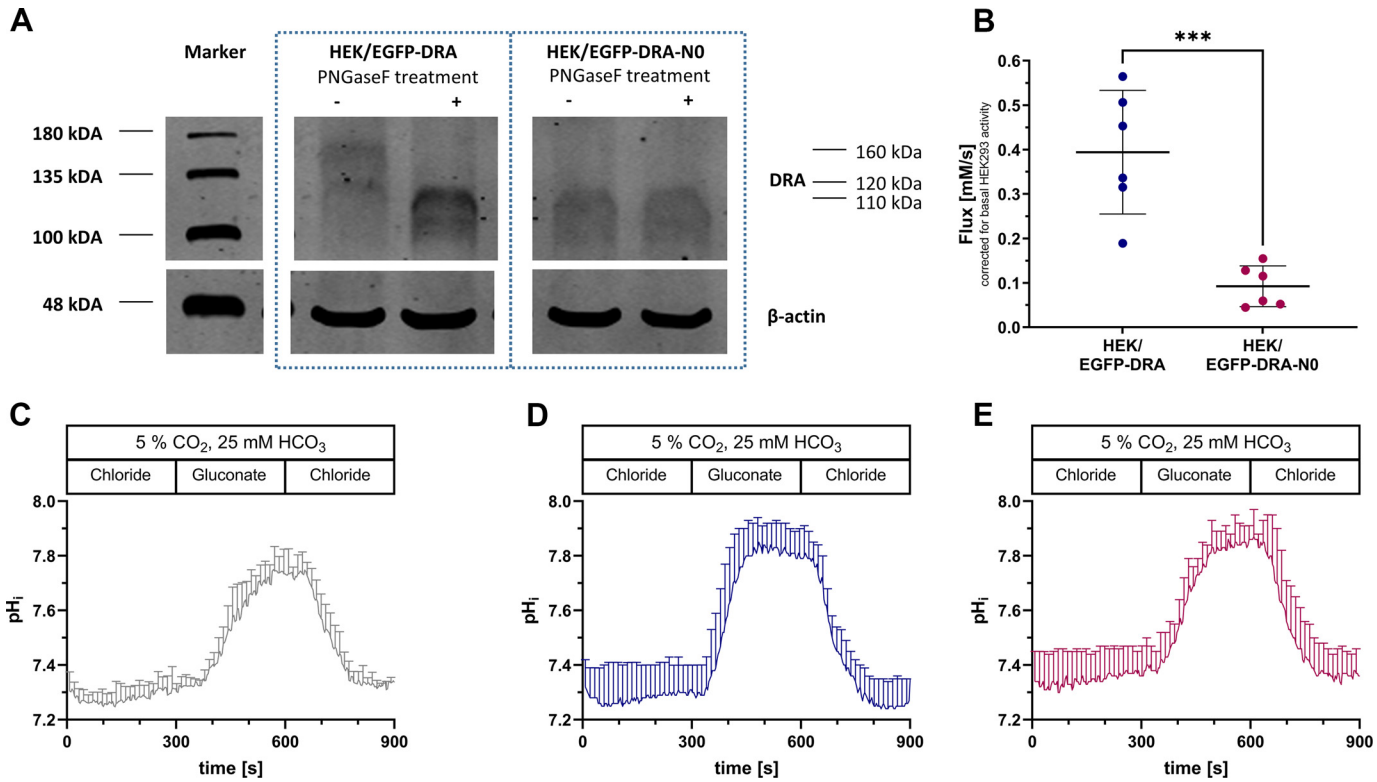

Figure 1. HEK/EGFP-DRA expresses complex *N*-glycosylated DRA and core/hybrid *N*-glycosylated DRA, whereas HEK/EGFP-DRA-N0 expresses non-*N*-glycosylated DRA, which significantly reduces transport activity. *A*: cell lysates were subjected to Western blot analysis both natively (−) and after treatment with PNGaseF (+). The activity of nontransfected HEK cells (*C*), HEK/EGFP-DRA (*D*), and HEK/EGFP-DRA-N0 (*E*) was measured as changes in intracellular pH (pH_i) upon removal and readdition of extracellular chloride by BCECF fluorometry. Nonlinear curve fitting was applied and background-corrected bicarbonate flux (*B*) was calculated. Means ± SD, *t* test, ***$P < 0.001$, $n = 6$. DRA, downregulated in adenoma (SLC26A3); EGFP, enhanced green fluorescent protein.

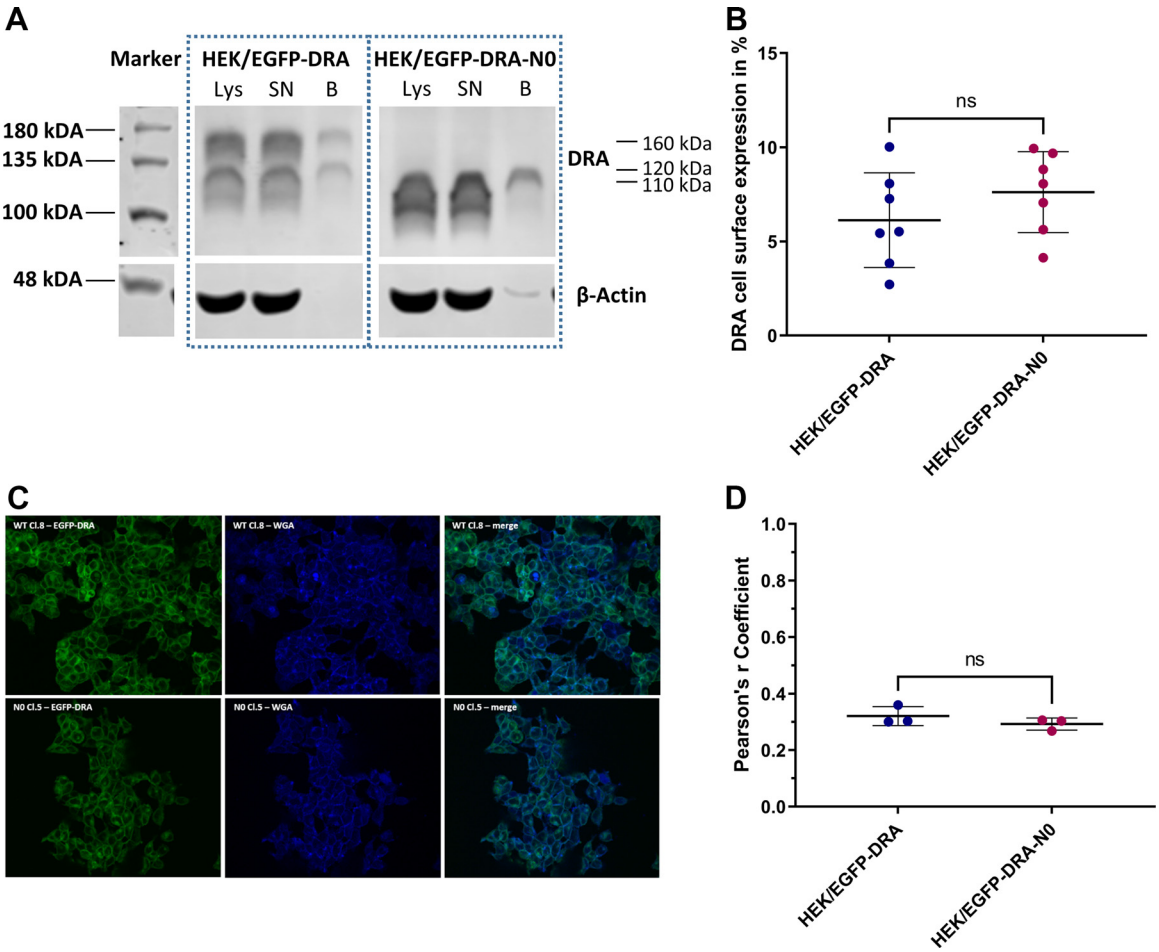

Figure 2. Cell surface expression, quantified by cell surface biotinylation and WGA colocalization, was measured for HEK/EGFP-DRA and HEK/EGFP-DRA-N0. The statistical analysis did not support a difference of abrogated *N*-glycosylation in the measured values. *A*: Western blot of a representative cell surface biotinylation experiment displays the cell lysate (Lys), the supernatant representing the nonsurface DRA (supernatant; SN), and the bead fraction representing the isolated surface DRA (beads; B) of HEK/EGFP-DRA and HEK/EGFP-DRA-N0. *B*: relative cell surface expression was quantified as percentage of isolated surface DRA relative to the cell lysate. Representative figures of colocalization of DRA with WGA as a plasma membrane marker protein (*C*) and quantification as Pearson's *r* coefficient (*D*). Means ± SD, *t* test, $n = 3$–7. DRA, downregulated in adenoma (SLC26A3); EGFP, enhanced green fluorescent protein; ns, not significant; WGA, wheat germ agglutinin.

exhibiting no statistically significant difference ($n = 7$). Of note, there appeared to be no difference between the cell lysate and the surface fraction in the relative abundance of the 160 kDa and the 120 kDa band of EGFP-DRA. The complex *N*-glycosylated DRA comprised 52 ± 5% in the cell lysate and 41 ± 7% in the surface fraction.

Colocalization of the EGFP fluorescence of EGFP-DRA and EGFP-DRA-N0 with WGA staining as a PM marker was tested. Figure 2, *C* and *D*, demonstrates that WGA colocalizes with both EGFP-DRA and EGFP-DRA-N0. Quantitatively, both EGFP-DRA and EGFP-DRA-N0 moderately colocalized with WGA in the PM (Pearson's correlation coefficient 0.32 ± 0.1 for EGFP-DRA vs. 0.29 ± 0.1 for EGFP-DRA-N0, not significant, $n = 3$). The statistical analysis failed to detect a difference in the measured values.

Thus, differences in relative cell surface expression are not the cause of the decreased activity of EGFP-DRA-N0. Furthermore, it appears that complex *N*-glycosylation does not affect incorporation into the PM, as the level of complex *N*-glycosylation in total protein lysate is comparable with that of the surface fraction.

Wild-Type DRA and *N*-Glycosylation Deficient DRA Are Present in Plasma Membrane-Derived Lipid Rafts

The reduction in activity of DRA in the absence of *N*-glycosylation appeared not be fully attributable to differing relative protein quantities present in the PM. Therefore, the impact of deficient *N*-glycosylation of DRA on incorporation into LRs was specifically tested.

LRs are detergent-resistant membranes, which float in low-density fractions when separated on a sucrose-gradient. Homogenates of HEK/EGFP-DRA and HEK/EGFP-DRA-N0 cells were subjected to a 5%/30%/40% sucrose gradient (Fig. 3*A*). Fractions 4 and 5 (F4 and F5 in Fig. 3*A*) at the interface between the 5% and 30% sucrose cushions were identified as the fractions containing LRs, as the majority of the LR marker flotillin was found in these fractions. Both EGFP-DRA and EGFP-DRA-N0 were detected in the LR containing fractions. Of note, in these LR fractions complex *N*-glycosylated EGFP-DRA migrating at 160 kDa appeared moderately overrepresented with 84% compared with the cell homogenate (Lys in Fig. 3*A*), where it comprised 48%.

Since sucrose gradient floatation addresses the entire LR pool of the cell, we subsequently measured the amount of DRA specifically present in PM-LRs. EGFP-DRA and EGFP-DRA-N0 were both found to be incorporated into PM-LRs (Fig. 3*B*) and were quantified relative to total EGFP-DRA or EGFP-DRA-N0 (Fig. 3*C*; EGFP-DRA 0.9 ± 0.1%, EGFP-DRA-N0: 0.6 ± 0.2%, not significant, $n = 3$). The statistical analysis did not support a difference in the measured values. This suggests that deficient *N*-glycosylation of DRA does not have an impact on the expression of DRA in PM-derived LRs. Of note, there appeared to be no difference in the relative abundance of the 160 kDa and 120 kDa bands of EGFP-DRA in the PM-LR fraction compared with the cell lysate (Fig. 3*B*; cell lysate 50 ± 6% vs. PM-LRs 53 ± 17%).

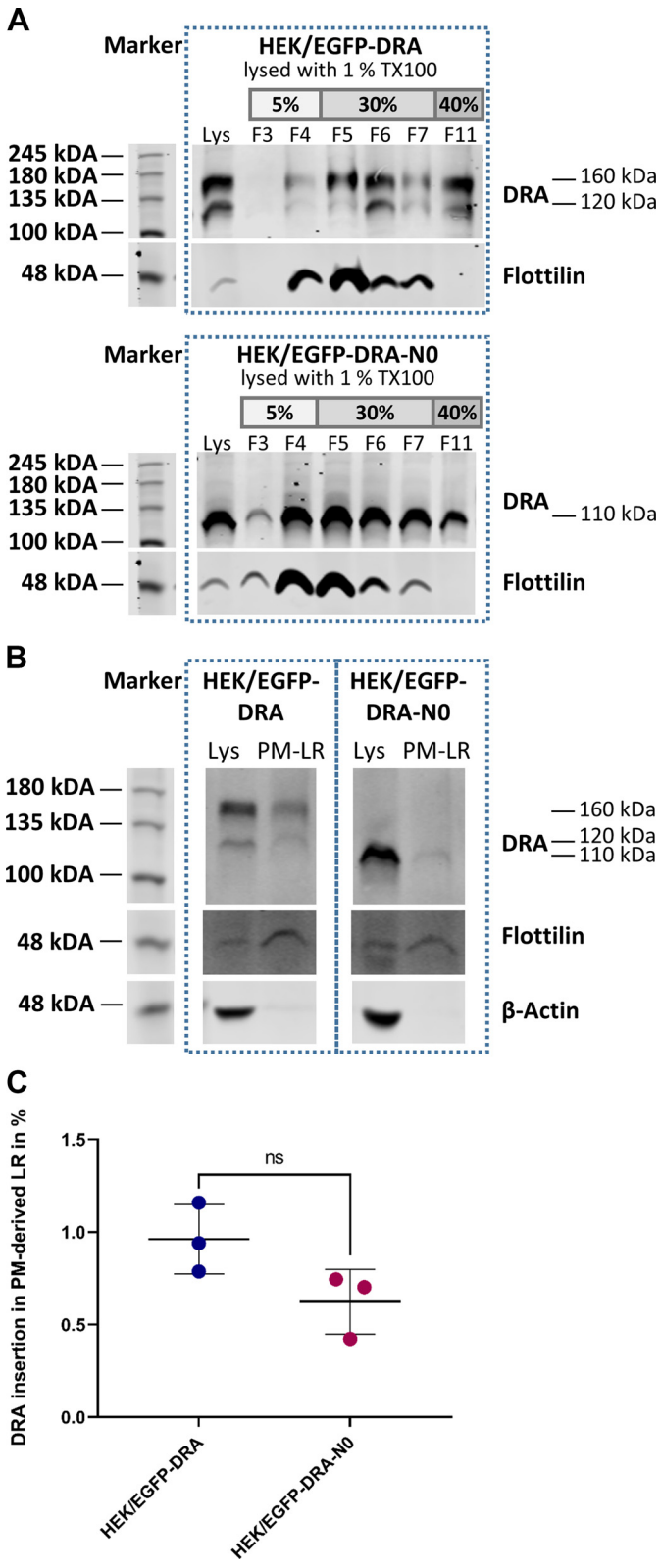

Absolute DRA Quantification

Absolute quantification of DRA was conducted by LC-MS/MS analysis of the proteospecific surrogate peptide LIDAVGFSPLR (amino acids 556–566 of human DRA) applying stable isotope-labeled standards and the FASP method. Measured DRA amounts were normalized to the protein content of the cell fractions analyzed (Fig. 4). In the total protein lysate, 8.0 ± 2.5 pmol/mg of EGFP-DRA was detected, which was significantly reduced to 3.5 ± 1.4 pmol/mg for EGFP-DRA-N0 ($P = 0.001$, $n = 7$). The same effect was observed in the PM showing significantly lower expression of EGFP-DRA-N0 (7.6 ± 2.0 pmol/mg) compared with EGFP-DRA (11.8 ± 2.1 pmol/mg; $P = 0.0021$, $n = 7$) and also in PM-LRs, where EGFP-DRA-N0 concentration was also significantly lower than the concentration of EGFP-DRA (EGFP-DRA-N0: 6.8 ± 3.0 pmol/mg vs. EGFP-DRA: 12.3 ± 2.3 pmol/mg; $P = 0.0002$, $n = 6$ or 7).

Taken together, absolute DRA protein concentrations were lowered by 57% in the protein lysate, 34% in the PM, and 45% in PM-LRs in EGFP-DRA-N0 versus EGFP-DRA.

Glycosylated DRA Structure

Due to the high structural homology of the members of the SLC26 family, DRA is likely suitable for accurate predictions with AlphaFold3 (AF3). To this end, structures of the glycosylated DRA dimer were predicted using the AF3 server. Glycosylations were added to N153, N161, and N164 from the extracellular loop of the transport domain, between transmembrane helices 3 and 4 (Fig. 5*A*). According to the vertical translation of the transport domain relative to the scaffold domain, 17 of the 30 predicted structures were classified as inward-facing, and 13 as outward-facing. Inward- and outward-facing structures exhibited an average vertical shift of ~4 Å (Fig. 5*B*). The predicted glycosylations exhibited a diverse set of conformations, which is indicative of

Figure 3. HEK/EGFP-DRA and HEK/EGFP-DRA-N0 are associated with lipid rafts prepared from whole cell homogenates and specifically isolated as plasma membrane lipid rafts. The statistical analysis did not support a difference of abrogated *N*-glycosylation in the measured values of the relative incorporations of DRA in plasma membrane lipid rafts. *A*: representative Western blot of sucrose gradient fractionation of whole cell homogenates with the cell lysate (Lys), fractions 3–7 (F3–F7) and fraction 11 (F11). Flottilin identifies F4 and F5 as lipid raft fractions. DRA and DRA-N0 are present in lipid rafts. *B*: representative Western blot of plasma membrane-derived lipid rafts isolated using the Minute PM-Derived Lipid Raft Isolation Kit and subjected to Western blot analysis with the cell lysate (Lys) and isolated plasma membrane-derived lipid rafts (PM-LRs). DRA and DRA-N0 are present in PM-LRs. *C*: quantification of three experiments as shown in *B*. Means ± SD, *t* test, $n = 3$. DRA, downregulated in adenoma (SLC26A3); EGFP, enhanced green fluorescent protein; ns, not significant.

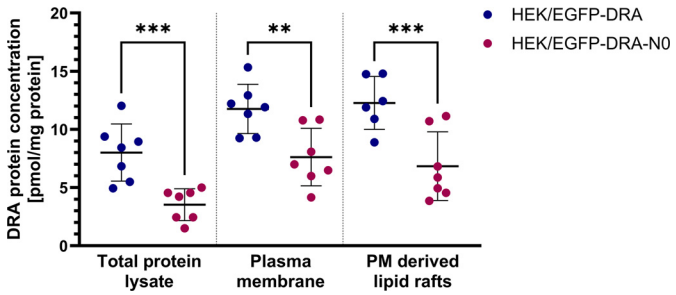

Figure 4. Absolute quantification of DRA by LC-MS/MS analysis of the proteospecific surrogate peptide LIDAVGFSPLR revealed significantly reduced absolute levels of DRA (pmol/mg protein) of HEK/EGFP-DRA-N0 in the total protein lysate, plasma membrane, and plasma membrane-derived lipid rafts compared with HEK/EGFP-DRA. Means ± SD, *t* test, $^{**}P < 0.01$, $^{***}P < 0.001$, $n = 6$ or 7. DRA, downregulated in adenoma (SLC26A3); EGFP, enhanced green fluorescent protein; LC-MS/MS, liquid chromatography-tandem mass spectrometry.

heightened dynamics, and sampled a substantial area on the extracellular surface [Fig. 5*C*, side-view (*top*), top-down view (*bottom*)]. The area sampled by the glycosylations exhibited a dependence on the relative conformations of the scaffold- and transport domains, that is, inward- and outward-facing (Fig. 5*C*, *bottom*).

To derive a potential mechanism-of-action for the observed glycosylation-enhanced transport activity, the contacts between the glycans and the protein backbone were evaluated. The predicted structures of DRA exhibited a conformational dependence on the number of interdomain interactions between the glycans. Though three predictions of the inward-facing state exhibited zero contacts, it was nevertheless associated with a significantly higher number of interdomain contacts than the outward-facing state (Fig. 5*D*; $P = 0.03$). The evaluated contacts come from the transport domain, reaching the apposed scaffold domain (Fig. 5*E*). These data suggest that the presence of glycans favors the inward-facing state.

DISCUSSION

Many proteins of the large SLC family of transmembrane proteins undergo *N*-glycosylation, which may affect their cellular activity, stability, or localization (17). NHE3 and CFTR, both working in close conjunction with DRA, also possess potential *N*-glycosylation sites (3, 32). NHE3 appears to be generally not *N*-glycosylated, with some species-specific exceptions (33). In contrast, NHE1 mature glycosylation determines polarized trafficking to the basolateral plasma membrane (34). *N*-glycosylation of CFTR has a critical impact on its folding and stability (32). Meanwhile, DRA is known to be *N*-glycosylated and expressed as both hybrid *N*-glycosylated and complex *N*-glycosylated forms (18, 19). The present study reveals a 70% decreased transport activity of the glycosylation-deficient DRA-N0 expressed in HEK cells. Previous studies by Hayashi et al. (18) and Rapp et al. (20) have shown that deficient *N*-glycosylation decreases DRA activity by 12.5% and 57%, respectively. Statistical analysis of surface biotinylation or WGA colocalization experiments does not support an effect of abrogated *N*-glycosylation on the relative surface expression of DRA. These findings corroborate the study of Rapp et al. (20), also showing no influence of *N*-glycosylation on surface expression in HEK cells and contrast with the study by Hayashi et al. (18) reporting a (nonsignificant) decrease in cell surface expression of *N*-glycosylation-deficient DRA in CHO cells. Furthermore, the proportion of complex *N*-glycosylated DRA to hybrid *N*-glycosylated DRA in the PM was not different from that in the lysate, indicating that complex *N*-glycosylated DRA is not favored for trafficking to the cell surface.

In a previous study, we (13) and in a recent study, Tse et al. (21) have realized that the complex *N*-glycosylated form of DRA is highly prevalent in LR fractions. Disruption of LRs using MβCD reduces DRA activity in HEK cells by 39% (13), while stimulation of DRA transport activity is associated with increased localization in LRs (21, 35). DRA insertion into LRs occurs via the PI3kinase-dependent exocytosis pathway and is facilitated by its interaction with PDZ adaptor proteins (13). In general, protein palmitoylation, the size of the transmembrane domain, and the TMD surface area are considered important factors for LR association (36, 37), but additional evidence suggests that *N*-glycosylation of a protein may also affect LR association (22–24). Based on these considerations, it was important to test whether the glycosylation of DRA influences its distribution in LRs and the nonraft fraction of the PM. To this end, isolation of whole-cell LRs by sucrose gradient fractionation appeared to show a shift toward complex *N*-glycosylated DRA in the isolated LR fractions, as reported before (13, 21). But DRA-N0 was also present in whole-cell LRs. As LRs are not restricted to the PM, PM-LRs were specifically isolated. By Western blot, both DRA and DRA-N0 were detected in the PM-LRs, but the statistical analysis failed to indicate a difference in the measured values of percentage incorporation into PM-LRs. Moreover, DRA did not exhibit a preference for the complex *N*-glycosylated form in PM-LR.

We also used absolute quantification of DRA by targeted quantitative proteomics, a technique that allows the concentration of a target protein (i.e., DRA or DRA-N0) to be determined down to a range of picomoles per milligram of protein in the cell fraction under study. In the cell lysate, this revealed a 57% reduced expression level of DRA-N0 compared with DRA. Furthermore, it showed a significant decrease of 34% in the PM and of 45% in PM-LRs. Although the reduced expression levels may account for some decline in activity, the 70% loss of total cellular transport activity cannot be entirely attributed to the 34% and 45% reduced presence of DRA-N0 in the PM or PM-LRs, respectively. Taken together, this indicates that *N*-glycosylation is not required for the effective insertion of DRA into PM and PM-LRs. Furthermore, this suggests that *N*-glycosylation of DRA affects the specific activity of the transporter. To this end, anion selectivity and stability have already been ruled out as potential mechanisms (18, 20). Thus, the effects of *N*-glycosylation of DRA on its molecular structure were evaluated using AlphaFold3 to predict the three-dimensional structure of DRA, including covalently bound "complex *N*-glycans," which has not been done before.

The predicted structures revealed multiple conformations of the glycans as well as DRA in both inward-facing and outward-facing states. The glycans, which are covalently bound to the transport domain, mediate various

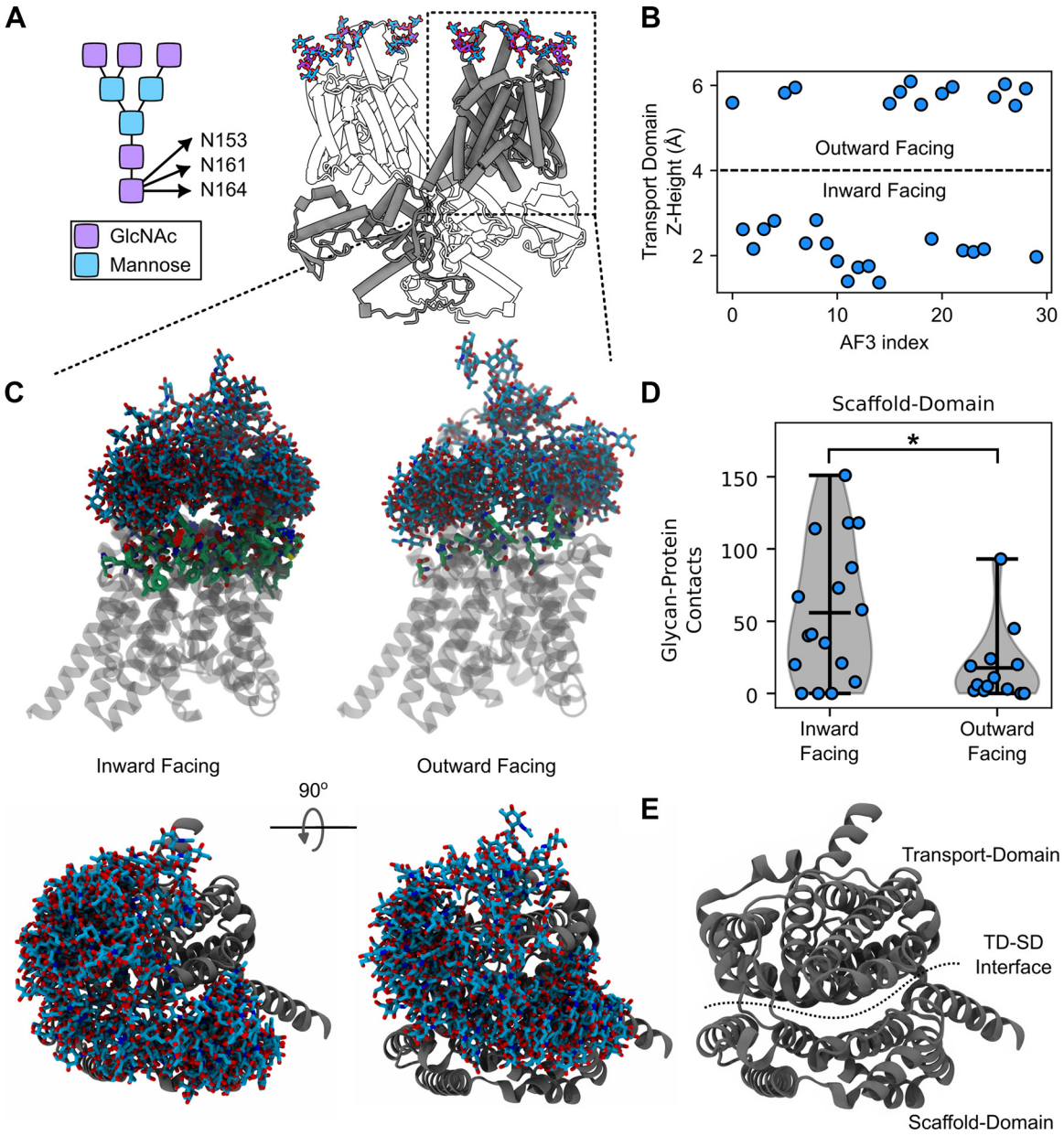

Figure 5. AlphaFold3 (AF3)-predicted structures of glycosylated DRA. *A*: schematic of the "complex *N*-glycan" used for structure prediction (*left*), and representative predicted structure (*right*) showing the domain-swapped dimer, and extracellular *N*-glycosylations of the transport domain. *B*: evaluating conformational heterogeneity predictions by measuring the *z*-component of the difference in centers of geometry between the transport (TD) and scaffold domain (SD)—separating inward-from outward-facing. *C*: visualization of the conformation-dependent, glycan-mediated interdomain contacts: protein (gray, transparent), glycans (blue), and scaffold domain-interacting residues (green) (*top*), visualization of the 90° rotated TMD exhibiting conformational dependence on extracellular surface coverage (*bottom*). The protein visualizations are a composite of all predicted structures (inward-facing, 17 structures; outward-facing, 13 structures). *D*: interdomain glycan-scaffold contacts, calculated from each predicted structure (*$P < 0.05$). *E*: transmembrane domain of a DRA protomer, from the extracellular perspective. Images were rendered using VMD and ChimeraX. DRA, downregulated in adenoma (SLC26A3); TMD, transmembrane domain.

interdomain contacts to the scaffold domain. Notably, the number of interdomain contacts was higher in the inward-facing state, indicating that the presence of glycans favors this conformation. In SLC26 anion antiporters, substrate transport across the membrane involves an elevator-transport mechanism wherein a transport domain makes a rotational-translational motion relative to a static scaffold domain—alternately exposing the anion-binding pocket to the intra- and extracellular environments (12). In many transport proteins, substrate release from the inward-facing state to the cytoplasm is the rate-limiting step for transport activity (38, 39). Thus, stabilization of the inward-facing state by glycans could facilitate anion transport. Such a model is also compatible with our previous findings that DRA has similar affinities to chloride and bicarbonate and thus transport is to a large degree determined by the different relative concentrations of both anions intra- and extracellularly (25).

To date, no mutation causing CLD has been identified that directly affects DRA glycosylation sites (40). However, some DRA mutants do not exhibit complex *N*-glycosylation, as illustrated by the I544 mutant, which is expressed in the plasma membrane but is nonactive due to its direct effect on the STAS domain, which is crucial for the transport activity of DRA (20, 41). The significance of the lack of complex *N*-glycosylation of DRA in vivo remains to be elucidated.

As a tool to quantify DRA absolutely, we have used LC-MS/MS-based targeted quantitative proteomics. Other methods for the detection of individual proteins, such as immunoblotting or immunohistochemistry, rely on antibody binding and only allow for semiquantitative measurements. Mass spectrometry-based targeted proteomics overcomes this limitation by directly detecting proteospecific peptides as surrogates for the target protein. Absolute quantification was achieved by using stable-isotope-labeled peptides as internal standards (42, 43). The method also allows for the quantification of several target proteins in the same sample, which are normalized to the same standard, usually the protein concentration in the cell fraction under study. Given the variability in protein composition across different subcellular compartments and the fact that cell and membrane fractionation is typically based on enrichment rather than quantitative preparation, it becomes evident that the concentration of one target protein determined by LC-MS/MS-based quantitative proteomics may not be compared between various compartments (i.e., fractions) under study. Nonetheless, the molar stoichiometry of two or more proteins in the same sample can be quantified. This will be an important improvement when studying the functional and structural coupling of transporters in a given cellular compartment or membrane fraction, as it is proposed for DRA with NHE3 and/or CFTR. For the current study, this does not apply as HEK cells do not express NHE3 and CFTR.

Taken together, our experimental data indicate that glycosylation does not influence DRA insertion into and retrieval from the PM and PM-LRs. Instead, molecular modeling predicts that complex *N*-glycans mediate interactions between the transport and the scaffold domain, favoring the inward-facing state and thereby potentially allowing more efficacious anion transport.

DATA AVAILABILITY

Data will be made available upon reasonable request.

SUPPLEMENTAL MATERIAL

Supplemental Fig. S1: https://doi.org/10.6084/m9.figshare.28497758.v1.

ACKNOWLEDGMENTS

Graphical abstract made with a licensed version of BioRender.com.

GRANTS

The mass spectrometric analysis of this project was supported by funding from the German Research Foundation (Project Number: 505943254) to S.O. This work was supported by the German Research Foundation as parts of the Research Unit FOR 5046 (Project Number: 426950122) to J.-P.M. (Project P2), to E.R.G. (Project P1), and to I.W. and G.L. (Project P5). The authors gratefully acknowledge computing time on the supercomputer JURECA (1) at Forschungszentrum Jülich under Grant No. jara0177.

DISCLOSURES

No conflicts of interest, financial or otherwise, are declared by the authors.

AUTHOR CONTRIBUTIONS

S.A., B.G.H., J.-P.M., E.R.G., I.W., and G.L. conceived and designed research; S.A., F.-S.B., B.G.H., and S.O. performed experiments; S.A., F.-S.B., B.G.H., and S.O. analyzed data; S.A., J.-N.T., F.-S.B., B.G.H., J.-P.M., I.W., and G.L. interpreted results of experiments; S.A. and B.G.H. prepared figures; S.A., J.-N.T., B.G.H., and G.L. drafted manuscript; S.O., J.-P.M., E.R.G., I.W., and G.L. edited and revised manuscript; S.A., J.-N.T., F.-S.B., B.G.H., S.O., J.-P.M., E.R.G., I.W., and G.L. approved final version of manuscript.

REFERENCES

1. **Seidler U**, **Nikolovska K.** Slc26 family of anion transporters in the gastrointestinal tract: expression, function, regulation, and role in disease. *Compr Physiol* 9: 839–872, 2019. doi:10.1002/cphy.c180027.
2. **Höglund P**, **Haila S**, **Socha J**, **Tomaszewski L**, **Saarialho-Kere U**, **Karjalainen-Lindsberg ML**, **Airola K**, **Holmberg C**, **de la Chapelle A**, **Kere J.** Mutations of the Down-regulated in adenoma (DRA) gene cause congenital chloride diarrhoea. *Nat Genet* 14: 316–319, 1996. doi:10.1038/ng1196-316.
3. **Zizak M**, **Cavet ME**, **Bayle D**, **Tse CM**, **Hallen S**, **Sachs G**, **Donowitz M.** Na^+/H^+ exchanger NHE3 has 11 membrane spanning domains and a cleaved signal peptide: topology analysis using in vitro transcription/translation. *Biochemistry* 39: 8102–8112, 2000. doi:10.1021/bi000870t.
4. **Schweinfest CW**, **Spyropoulos DD**, **Henderson KW**, **Kim JH**, **Chapman JM**, **Barone S**, **Worrell RT**, **Wang Z**, **Soleimani M.** slc26a3 (dra)-deficient mice display chloride-losing diarrhea, enhanced colonic proliferation, and distinct up-regulation of ion transporters in the colon. *J Biol Chem* 281: 37962–37971, 2006. doi:10.1074/jbc.M607527200.
5. **Knickelbein R**, **Aronson PS**, **Schron CM**, **Seifter J**, **Dobbins JW.** Sodium and chloride transport across rabbit ileal brush border. II. Evidence for Cl-HCO3 exchange and mechanism of coupling. *Am J Physiol Gastrointest Liver Physiol* 249: G236–G245, 1985. doi:10.1152/ajpgi.1985.249.2.G236.
6. **Lamprecht G**, **Heil A**, **Baisch S**, **Lin-Wu E**, **Yun CC**, **Kalbacher H**, **Gregor M**, **Seidler U.** The down regulated in adenoma (dra) gene product binds to the second PDZ domain of the NHE3 kinase A regulatory protein (E3KARP), potentially linking intestinal Cl-/HCO3- exchange to $Na+/H+$ exchange. *Biochemistry* 41: 12336–12342, 2002. doi:10.1021/bi0259103.
7. **Musch MW**, **Arvans DL**, **Wu GD**, **Chang EB.** Functional coupling of the downregulated in adenoma Cl-/base exchanger DRA and the apical $Na+/H+$ exchangers NHE2 and NHE3. *Am J Physiol Gastrointest Liver Physiol* 296: G202–G210, 2009. doi:10.1152/ajpgi.90350.2008.
8. **Talbot C**, **Lytle C.** Segregation of Na/H exchanger-3 and Cl/HCO3 exchanger SLC26A3 (DRA) in rodent cecum and colon. *Am J Physiol Gastrointest Liver Physiol* 299: G358–G367, 2010. doi:10.1152/ajpgi.00151.2010.
9. **Bachmann O**, **Seidler U.** News from the end of the gut–how the highly segmental pattern of colonic HCO_3^- transport relates to absorptive function and mucosal integrity. *Biol Pharm Bull* 34: 794–802, 2011. doi:10.1248/bpb.34.794.
10. **Donowitz M**, **Sarker R**, **Lin R**, **McNamara G**, **Tse CM**, **Singh V.** Identification of intestinal NaCl absorptive-anion secretory cells:

potential functional significance. *Front Physiol* 13: 892112, 2022. doi:10.3389/fphys.2022.892112.

11. **Kini A**, **Singh AK**, **Riederer B**, **Yang I**, **Tan X**, **di Stefano G**, **Tan Q**, **Xiao F**, **Xia W**, **Suerbaum S**, **Seidler U.** Slc26a3 deletion alters pH-microclimate, mucin biosynthesis, microbiome composition and increases the TNFα expression in murine colon. *Acta Physiol (Oxf)* 230: e13498, 2020. doi:10.1111/apha.13498.
12. **Geertsma ER**, **Oliver D.** SLC26 anion transporters. *Handb Exp Pharmacol* 283: 319–360, 2024. doi:10.1007/164_2023_698.
13. **Lissner S**, **Nold L**, **Hsieh CJ**, **Turner JR**, **Gregor M**, **Graeve L**, **Lamprecht G.** Activity and PI3-kinase dependent trafficking of the intestinal anion exchanger downregulated in adenoma depend on its PDZ interaction and on lipid rafts. *Am J Physiol Gastrointest Liver Physiol* 299: G907–G920, 2010. doi:10.1152/ajpgi.00191.2010.
14. **Tse CM**, **Yin J**, **Singh V**, **Sarker R**, **Lin R**, **Verkman AS**, **Turner JR**, **Donowitz M.** cAMP stimulates SLC26A3 activity in human colon by a CFTR-dependent mechanism that does not require CFTR activity. *Cell Mol Gastroenterol Hepatol* 7: 641–653, 2019. doi:10.1016/j.jcmgh.2019.01.002.
15. **Lissner S**, **Hsieh CJ**, **Nold L**, **Bannert K**, **Bodammer P**, **Sultan A**, **Seidler U**, **Graeve L**, **Lamprecht G.** The PDZ-interaction of the intestinal anion exchanger downregulated in adenoma (DRA; SLC26A3) facilitates its movement into Rab11a-positive recycling endosomes. *Am J Physiol Gastrointest Liver Physiol* 304: G980–G990, 2013. doi:10.1152/ajpgi.00132.2012.
16. **Bannert K**, **Berlin P**, **Reiner J**, **Lemcke H**, **David R**, **Engelmann R**, **Lamprecht G.** SNX27 regulates DRA activity and mediates its direct recycling by PDZ-interaction in early endosomes at the apical pole of Caco2 cells. *Am J Physiol Gastrointest Liver Physiol* 318: G854–G869, 2020. doi:10.1152/ajpgi.00374.2019.
17. **Pedersen NB**, **Carlsson MC**, **Pedersen SF.** Glycosylation of solute carriers: mechanisms and functional consequences. *Pflugers Arch* 468: 159–176, 2016. doi:10.1007/s00424-015-1730-4.
18. **Hayashi H**, **Yamashita Y.** Role of N-glycosylation in cell surface expression and protection against proteolysis of the intestinal anion exchanger SLC26A3. *Am J Physiol Cell Physiol* 302: C781–C795, 2012. doi:10.1152/ajpcell.00165.2011.
19. **Li J**, **Xia F**, **Reithmeier RAF.** N-glycosylation and topology of the human SLC26 family of anion transport membrane proteins. *Am J Physiol Cell Physiol* 306: C943–C960, 2014. doi:10.1152/ajpcell.00030.2014.
20. **Rapp CL**, **Li J**, **Badior KE**, **Williams DB**, **Casey JR**, **Reithmeier RAF.** Role of N-glycosylation in the expression of human SLC26A2 and A3 anion transport membrane glycoproteins[1]. *Biochem Cell Biol* 97: 290–306, 2019. doi:10.1139/bcb-2018-0139.
21. **Tse CM**, **Zhang Z**, **Lin R**, **Sarker R**, **Donowitz M**, **Singh V.** The air-liquid interface reorganizes membrane lipids and enhances the recruitment of Slc26a3 to lipid-rich domains in human colonoid monolayers. *Int J Mol Sci* 24: 8273, 2023. doi:10.3390/ijms24098273.
22. **Chen G**, **Howe AG**, **Xu G**, **Fröhlich O**, **Klein JD**, **Sands JM.** Mature N-linked glycans facilitate UT-A1 urea transporter lipid raft compartmentalization. *FASEB J* 25: 4531–4539, 2011. doi:10.1096/fj.11-185991.
23. **Morenilla-Palao C**, **Pertusa M**, **Meseguer V**, **Cabedo H**, **Viana F.** Lipid raft segregation modulates TRPM8 channel activity. *J Biol Chem* 284: 9215–9224, 2009. doi:10.1074/jbc.M807228200.
24. **Pagano M**, **Clynes MA**, **Masada N**, **Ciruela A**, **Ayling LJ**, **Wachten S**, **Cooper DMF.** Insights into the residence in lipid rafts of adenylyl cyclase AC8 and its regulation by capacitative calcium entry. *Am J Physiol Cell Physiol* 296: C607–C619, 2009. doi:10.1152/ajpcell.00488.2008.
25. **Lamprecht G**, **Baisch S**, **Schoenleber E**, **Gregor M.** Transport properties of the human intestinal anion exchanger DRA (down-regulated in adenoma) in transfected HEK293 cells. *Pflugers Arch* 449: 479–490, 2005. doi:10.1007/s00424-004-1342-x.
26. **Lamprecht G**, **Schaefer J**, **Dietz K**, **Gregor M.** Chloride and bicarbonate have similar affinities to the intestinal anion exchanger DRA (down regulated in adenoma). *Pflugers Arch - Eur J Physiol* 452: 307–315, 2006. doi:10.1007/s00424-006-0049-6.
27. **Wiśniewski JR**, **Zougman A**, **Nagaraj N**, **Mann M.** Universal sample preparation method for proteome analysis. *Nat Methods* 6: 359–362, 2009. doi:10.1038/nmeth.1322.
28. **Drozdzik M**, **Busch D**, **Lapczuk J**, **Müller J**, **Ostrowski M**, **Kurzawski M**, **Oswald S.** Protein abundance of clinically relevant drug transporters in the human liver and intestine: a comparative analysis in paired tissue specimens. *Clin Pharmacol Ther* 105: 1204–1212, 2019. doi:10.1002/cpt.1301.
29. **Abramson J**, **Adler J**, **Dunger J**, **Evans R**, **Green T**, **Pritzel A**, **et al.** Accurate structure prediction of biomolecular interactions with AlphaFold 3. *Nature* 636: E4, 2024. doi:10.1038/s41586-024-08416-7.
30. **Humphrey W**, **Dalke A**, **Schulten K.** VMD: visual molecular dynamics. resource available. *J Mol Graph* 14: 33–38, 1996. doi:10.1016/0263-7855(96)00018-5.
31. **Pettersen EF**, **Goddard TD**, **Huang CC**, **Couch GS**, **Greenblatt DM**, **Meng EC**, **Ferrin TE.** UCSF Chimera–a visualization system for exploratory research and analysis. *J Comput Chem* 25: 1605–1612, 2004. doi:10.1002/jcc.20084.
32. **Glozman R**, **Okiyoneda T**, **Mulvihill CM**, **Rini JM**, **Barriere H**, **Lukacs GL.** N-glycans are direct determinants of CFTR folding and stability in secretory and endocytic membrane traffic. *J Cell Biol* 184: 847–862, 2009. doi:10.1083/jcb.200808124.
33. **Bizal GL**, **Howard RL**, **Bookstein C**, **Rao MC**, **Chang EB**, **Soleimani M.** Glycosylation of the Na + /H + exchanger isoform NHE-3 is species specific. *J Lab Clin Med* 128: 304–312, 1996. doi:10.1016/S0022-2143(96)90032-3.
34. **Coupaye-Gerard B**, **Bookstein C**, **Duncan P**, **Chen XY**, **Smith PR**, **Musch M**, **Ernst SA**, **Chang EB**, **Kleyman TR.** Biosynthesis and cell surface delivery of the NHE1 isoform of Na + /H + exchanger in A6 cells. *Am J Physiol Cell Mol Physiol* 271: C1639–C1645, 1996. doi:10.1152/ajpcell.1996.271.5.C1639.
35. **Saksena S**, **Tyagi S**, **Goyal S**, **Gill RK**, **Alrefai WA**, **Ramaswamy K**, **Dudeja PK.** Stimulation of apical $Cl^-/HCO_3^-(OH^-)$ exchanger, SLC26A3 by neuropeptide Y is lipid raft dependent. *Am J Physiol Gastrointest Liver Physiol* 299: G1334–G1343, 2010. doi:10.1152/ajpgi.00039.2010.
36. **Diaz-Rohrer BB**, **Levental KR**, **Simons K**, **Levental I.** Membrane raft association is a determinant of plasma membrane localization. *Proc Natl Acad Sci USA* 111: 8500–8505, 2014. doi:10.1073/pnas.1404582111.
37. **Lorent JH**, **Diaz-Rohrer B**, **Lin X**, **Spring K**, **Gorfe AA**, **Levental KR**, **Levental I.** Structural determinants and functional consequences of protein affinity for membrane rafts. *Nat Commun* 8: 1219, 2017 [Erratum in *Nat Commun* 9: 1805, 2018]. doi:10.1038/s41467-017-01328-3.
38. **Oh S**, **Boudker O.** Kinetic mechanism of coupled binding in sodium-aspartate symporter GltPh. *eLife* 7: e37291, 2018. doi:10.7554/elife.37291.
39. **Huysmans GHM**, **Ciftci D**, **Wang X**, **Blanchard SC**, **Boudker O.** The high-energy transition state of the glutamate transporter homologue GltPh. *EMBO J* 40: e105415, 2021. doi:10.15252/embj.2020105415.
40. **Wedenoja S**, **Pekansaari E**, **Höglund P**, **Mäkelä S**, **Holmberg C**, **Kere J.** Update on SLC26A3 mutations in congenital chloride diarrhea. *Hum Mutat* 32: 715–722, 2011. doi:10.1002/humu.21498.
41. **Chernova MN**, **Jiang L**, **Shmukler BE**, **Schweinfest CW**, **Blanco P**, **Freedman SD**, **Stewart AK**, **Alper SL.** Acute regulation of the SLC26A3 congenital chloride diarrhoea anion exchanger (DRA) expressed in Xenopus oocytes. *J Physiol* 549: 3–19, 2003. doi:10.1113/jphysiol.2003.039818.
42. **Oswald S**, **Gröer C**, **Drozdzik M**, **Siegmund W.** Mass spectrometry-based targeted proteomics as a tool to elucidate the expression and function of intestinal drug transporters. *AAPS J* 15: 1128–1140, 2013. doi:10.1208/s12248-013-9521-3.
43. **Wenzel C**, **Drozdzik M**, **Oswald S.** Mass spectrometry-based targeted proteomics method for the quantification of clinically relevant drug metabolizing enzymes in human specimens. *J Chromatogr B Analyt Technol Biomed Life Sci* 1180: 122891, 2021. doi:10.1016/j.jchromb.2021.122891.